Differential and integrated cross sections for excitation to the 3*s*, 3*p*, and 3*d* states of atomic hydrogen by electron impact below the *n*=4 threshold

Philip L. Bartlett,[1] J. F. Williams,[2,3] Igor Bray,[1] A. G. Mikosza,[3] and Andris T. Stelbovics[1]
[1]*The ARC Centre for Antimatter-Matter Studies, Murdoch University, Perth 6150, Australia*
[2]*The ARC Centre for Antimatter-Matter Studies, University of Western Australia, Perth 6009, Australia*
[3]*Centre for Atomic, Molecular and Surface Physics, University of Western Australia, Perth 6009, Australia*
(Received 5 June 2006; published 10 August 2006)

Integrated cross sections for the electron-impact excitation of ground-state hydrogen to the 3*s*, 3*p*, and 3*d* final states have been calculated using propagating exterior complex scaling and convergent close-coupling methods at energies between the *n*=3 and 4 excitation thresholds. The calculations are in excellent agreement and demonstrate that exterior complex scaling methods can accurately reproduce the resonance structure and magnitude of the excitation cross sections below the ionization threshold. Measurements of the separate 3*s*, 3*p*, and 3*d* differential cross sections were made at 12.24 eV, and are consistent with both calculations within a total experimental uncertainty of about 35%.

DOI: 10.1103/PhysRevA.74.022714 PACS number(s): 34.80.Dp

I. INTRODUCTION

Over the past decade, the method of exterior complex scaling (ECS) has been successfully applied to several three-body problems, the most notable of which was the electron-impact ionization of hydrogen [1]. The ECS method solves the Schrödinger equation directly in coordinate space and gives *ab initio* solutions for *e*-H ionizing collisions in all kinematic domains. A recent variant of the ECS method, propagating exterior complex scaling (PECS) [2], has given significant insights into *e*-H ionizing collisions at energies approaching the ionization threshold [3,4], and has also given highly accurate integrated and differential scattering cross sections [2,5] and Stokes parameter calculations [6]. To date, however, all *e*-H calculations undertaken with ECS or PECS methods have been made at energies above the ionization threshold. The purpose of this paper is to investigate the PECS method *below* the ionization threshold, and present measurements and convergent close-coupling (CCC) results for excitation to the separate *n*=3 states at energies below the *n*=4 threshold.

The scattering wave functions below the ionization threshold differ significantly from those above ionization threshold, which affects the operation of the exterior complex scaling transformation. The ECS or PECS methods for *e*-H collisions apply this transformation

$$z(r) = \begin{cases} r, & r < R_0 \\ R_0 + (r - R_0)e^{i\theta}, & r \geqslant R_0 \end{cases} \quad (1)$$

separately to each electrons' radial coordinate (r_1 and r_2) near the outer edge of the calculation grids (R_0) so as to diminish exponentially all outgoing waves. At a small distance beyond R_0, the wave function can be assumed to be zero. Above the ionization threshold, the scattering wave function contains outgoing waves in all regions; near $r_1 = r_2$, this is predominantly due to ionization flux, and for $r_1 \ll r_2$ or $r_2 \ll r_1$ this is predominantly due to scattering processes. However, below the ionization threshold there is no possibility of double electron escape, and large sections of the scattering wave function near $r_1 = r_2 \to R_0$ will not contain outgoing waves. The adjacent regions where $0 \ll r_1 \ll r_2$ or $0 \ll r_2 \ll r_1$ will contain the flux for highly excited final states, but the energy of the scattered electron will be very low and the wavelength of the outgoing waves will be large. Hence the scattering wave function will diminish very slowly under ECS transformation in this region. In addition, the cross sections for excited states are very small, relative to the elastic channel, and significant resonant behavior is known to exist near the excitation thresholds. It is not clear whether exterior complex scaling methods can calculate *accurate* cross sections under these circumstances.

Several theoretical studies of the electron-impact excitation of ground-state hydrogen to the separate 3*s*, 3*p*, and 3*d* final states have been made at energies below the *n*=4 threshold. These were made using the *J*-matrix [7], algebraic variational [8], *R*-matrix [9,10], and *R*-matrix propagator [11] methods. It was suggested by Fon *et al.* [9] that the *J*-matrix calculations were not fully converged and that while the *R*-matrix calculations gave an accurate representation of resonance structure, they were 15% larger than their more accurate algebraic variational calculations. This was attributed to ionization continuum contributions that were neglected in the *R*-matrix calculations. As the variational calculations were not extended to the highly resonant region near the *n*=4 threshold, only the *R*-matrix propagator method of Dunseath *et al.* [11] has demonstrated both convergence *and* accurate cross sections near this threshold. Furthermore, no measurements have been reported for either integrated or differential cross sections in this region.

In this paper, we present PECS and CCC calculations of the integrated cross sections for electron-impact excitation of ground-state hydrogen to the separate 3*s*, 3*p*, and 3*d* states at energies between the *n*=3 and *n*=4 thresholds. In a previous paper [5], we gave separate 3*s*, 3*p*, and 3*d* measurements at energies above the ionization threshold, along with PECS and CCC calculations. The measurement technique, which proved to be extremely technically challenging, is also able to measure differential cross sections below the ionization threshold. Here, we present 3*s*, 3*p*, and 3*d* differential measurements at 12.24 eV, which provide support for our PECS and CCC calculations.

II. THEORETICAL METHODS

A. Propagating exterior complex scaling

The PECS method for calculating scattering wave functions for e-H collisions is described in detail in [2,12] and, while using markedly different numerical algorithms, is based upon the ECS method originally applied to e-H by Rescigno *et al.* [1].

In summary, the antisymmetrized scattering wave function is calculated on a finite grid in coordinate space with nonuniform spacing extending to R_0 a.u., where the coordinates are separately rotated by a fixed angle θ into the complex plane using the transformation given in Eq. (1). This transformation causes outgoing waves to diminish exponentially beyond R_0 and within a short distance (about one oscillation of the wave function) become effectively zero. The boundary condition for the scaled wave function is set to zero at this point ($R_{\max}$), and an essentially exact wave function is calculated using finite-difference methods and the known initial-state wave function. A propagating algorithm is used to "solve" one column of the grid at a time, rather than simultaneous solution of the entire grid, and proves to be computationally efficient.

A partial wave expansion reduces the dimensionality of the problem, and it was found that an iterative procedure could be used to solve the coupled partial waves [2]. This provides a dramatic computational saving over the simultaneous solution of the partial waves. This iterative coupling procedure becomes divergent as the incident-electron energy approaches the ionization threshold [3], due to strong electron correlation, and the coupled partial waves for each total angular momentum (L) and spin (S) must be solved simultaneously.

In the present study, below the ionization threshold, we found that the iterative coupling procedure *was* convergent, except at energies near resonances. At these energies the partial waves with L and S matching the resonance need simultaneous solution, while iterative coupling can be used for the remaining partial waves. Thus, the iterative coupling procedure provides a very significant computational saving, especially at energies closer to the $n=3$ threshold where there is little resonance structure.

PECS wave functions were calculated at 125 energies between 12.200 eV (0.8967 Ry) and 12.755 eV (0.9375 Ry, $n=4$ threshold), using finer energy spacing at higher energies where there is more structure. All calculations used the same grid spacing, grid size ($R_0=200$ a.u.), and complex scaling interval ($R_{\max}-R_0=20$ a.u.), apart from the 12.24 eV calculation where R_0 was extended to 300 a.u. to investigate radial convergence. Partial waves with $L\leqslant 5$ were included in all calculations.

One significant difference from near-threshold ionization calculations is the relatively small complex scaling interval required for convergence of the scattering cross sections. Above the ionization threshold, good convergence is obtained when the complex scaling interval ($R_{\max}-R_0$) is approximately one wavelength of an outgoing wave with energy equal to the excess energy. Noting that the rate of attenuation of the ECS transformation in Eq. (1) is proportional to the wavelength of the outgoing wave, a complex scaling interval of approximately 75 a.u. would be indicated for our lowest-energy calculation (0.1 eV above the $n=3$ threshold), but good convergence was obtained with a 20 a.u. interval. We believe that the relatively close proximity, and partial overlap, of the wave-function regions that contain flux for $n=2$ excitation, where the scattered electron has much higher energy, reduces the requirement for such large complex scaling intervals.

Once accurate scattering wave functions were calculated, the scattering cross sections were extracted using the surface integral method of [13] detailed in [2,12]. The partial-wave amplitude in this method is given by

$$f_j^{l_1 LS}(k_j) \sim \int dr_2 r_1^2 \phi_{n_j l_j}(r_2) \left[\frac{1}{r_1} \psi_{l_1 l_j}^{LS}(r_1, r_2) \frac{\partial}{\partial r_1} j_{l_1}(k_j r_1) - j_{l_1}(k_j r_1) \frac{\partial}{\partial r_1} \frac{1}{r_1} \psi_{l_1 l_j}^{LS}(r_1, r_2) \right], \tag{2}$$

where r_1 is arbitrarily taken to be the radial coordinate of the scattered electron, r_2 is the radial coordinate of the bound electron, $\phi_{n_j l_j}(r_2)$ is the hydrogen final-state radial wave function, $\psi_{l_1 l_j}^{LS}(r_1, r_2)$ is the calculated scattering wave function, and $j_{l_1}(k_j r_1)$ is the spherical Bessel function. This method uses an asymptotic form of the final-state wave function and the resultant cross sections converge with increasing r_1 to the asymptotic solution. The rate of convergence depends upon the final state of the target ($n_j l_j$) and the final momentum of the scattered electron (k_j), and hence influences the grid size R_0 required for the calculation.

The *raw* integrated cross sections at incident energy $E_0=12.24$ eV are shown in Fig. 1 for all open channels ($1s$, $2s$, $2p$, $3s$, $3p$, and $3d$), as a function of r_1. The elastic channel converges very quickly, while the $n_j=3$ states converge very slowly, which is directly related to the energy of the scattered electron. This energy is 12.24 eV for the elastic channel, giving cross sections stable to within 0.1% by $r_1=30$ a.u., while for $n_j=3$ it is very low (0.15 eV) and the cross sections have not fully converged by $r_1=300$ a.u. The magnitude of the oscillations in the cross sections diminishes with increasing r_1, the period of the oscillations is inversely related to the momentum of the scattered electron, and the cross sections converge as a function of $1/r_1$. The dashed lines in Fig. 1 show the best fit to the function

$$\sigma(r_1) = \bar{\sigma}(1 + a/r_1), \tag{3}$$

fitted between 50 and 300 a.u. This function accurately models the convergence behavior, and is used to calculate the asymptotic extrapolation $\bar{\sigma}$ given in this paper. R_0 can therefore be limited to 200 a.u. at lower energies without affecting accuracy. The effect of this extrapolation is not distinguishable above 0.92 Ry in the plots presented here, and we estimate that the standard error of the integrated cross sections is better than 3% (after extrapolation).

The convergence behavior exhibited by the cross sections below the ionization threshold is the same as that observed above ionization threshold, albeit with slower radial conver-

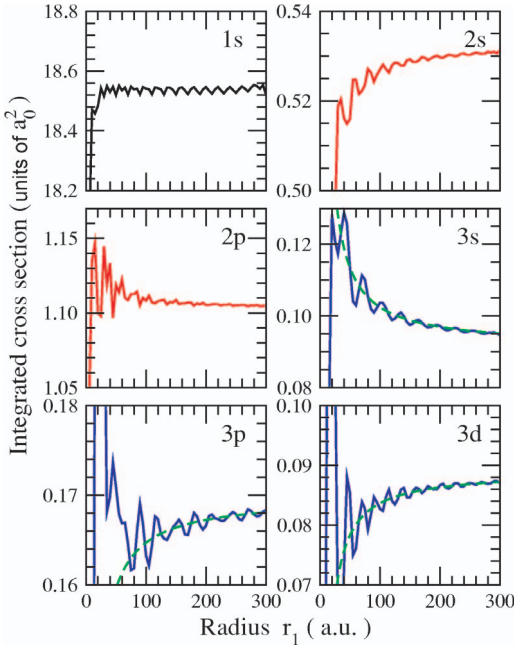

FIG. 1. (Color online) PECS elastic ($1s$) and excited final-state ($2s$, $2p$, $3s$, $3p$, and $3d$) cross-section calculations at $E_0=12.24$ eV, with respect to r_1 of the integral calculation in Eq. (2). Dashed lines for $n_j=3$ states show the best fit to a $1/r_1$ convergence estimate.

gence due to the much lower energy of the scattered electrons.

B. Convergent close coupling

We utilize the original Laguerre-based CCC method [14] in the present study. This has the advantage over the box-based method [15] in that higher positive-energy states are able to be obtained with fewer target states. In the box-based approach, the target-state momentum distribution is roughly linear, whereas in the Laguerre-based approach the momenta grow approximately exponentially. Given that we are interested in energies a little below the $n=4$ threshold, we need our calculations to accurately model highly excited states, and as always for H and He, we also need enough high positive-energy states to ensure that the target polarizability is well-reproduced.

The Laguerre basis has two parameters for each angular momentum l. These are the basis size N_l and the exponential fall-off parameter λ_l. These need to be chosen keeping in mind the energy and physical observables of interest. For each $0 \leqslant l \leqslant l_{\max}=4$ we took $N_l=25-l$ and $\lambda_l=2$. The first $(6-l)$ states have negative energy and the rest are positive, extending to in excess of 1 keV, and all of which are closed. Accordingly, we include in our calculations only the first $(18-l)$ states, leading to those above 40 eV being neglected. The resultant CCC calculation has 80 states and can be executed very efficiently at the many energies of interest in this paper.

III. EXPERIMENTAL METHOD

The apparatus is based on a crossed electron-atom beams geometry and the experimental method detects, in coincidence, the scattered energy-loss electrons and the radiated photons from the decay of the excited state. Those details have been described in a series of papers, traceable from Williams *et al.* [5] and references therein. The major experimental advance of that recent work was the separate identification of the excitation of the $3s$, $3p$, and $3d$ states at incident energies from 16.5 to 54 eV. Here the experimental challenge was the extension of that approach to an incident electron energy of 12.24 eV, and consequently the detection of the scattered electrons with an energy of 0.15 eV, i.e., just above the $n=3$ threshold of 12.09 eV. Those achievements were made as follows.

The incident energy of 12.24 eV was chosen as it is below all resonances associated with the $n=4$ level and just above the $n=3$ threshold resonances. The incident electron energy spread, selected by a cylindrical electrostatic 127° analyzer, was 0.1 eV at a full width at half-maximum of a near-Gaussian function. This width was selected as a compromise between good energy resolution, an incident electron beam current that produced a reasonable ratio of true-to-random signals, and ease of analysis of the scattered electron signals. The electron beam current was about 0.5 μA at 12.24 eV and 1 mm wide with an angular spread of about two degrees. The energy-loss scattered electrons were selected at angles from 30° to 150°, accelerated, and then dispersed in energy by a cylindrical electrostatic 127° analyzer onto a position-sensitive channel-plate detector. Such a detector makes the task of identifying an energy-loss spectrum easier and is more accurate than channeltron (i.e., integrated over position) detection. Because the incident energy was below the ionization threshold, the energy-loss spectrum did not contain a continuum energy spread and clearly showed the discrete loss peaks from the $n=2$ and 3 levels above a near-zero background. It was essential to maintain zero electric and magnetic fields and gradients in the electron-atom interaction region and the scattered electron flight. Other aspects of detecting low-energy electrons were given in [4,16].

The photons are selected by a cone of solid angle that generally was as large as possible, within the space remaining after the incident and scattered electron source and detector were positioned. The 656.2 nm photons were detected by an EMI 9883 photomultiplier tube and the Lyman photons by a microchannel plate stack with appropriate filters.

As in the earlier study [5], the $3s$, $3p$, and $3d$ components were identified via their lifetimes of 158, 5.3, and 15.5 ns, respectively, for which the time-zero reference was provided by the $n=3$ energy-loss electrons. Also the $3p$ (102.6 nm) photons were detected separately from the $2p$ (121.6 nm) photons by an indium ultrathin film low-pass wavelength filter [17]. The $3d$ photons were identified via the coincidence detection of the cascade $2p$ photons with the $n=3$ energy-loss electron. To minimize the effect of directly excited $2p$ photon signals, this coincidence detection was made in anticoincidence with the $n=2$ energy-loss electrons [17–19]. The energies at which the photon signals appeared allowed the effectiveness of the filters to be verified. The uv photons detected from the np levels with electron incident energies near threshold were as follows: only background molecular radiation at 10.0 eV, only Lyman-alpha photons at 11.0 eV, and both Lyman-alpha and Lyman-beta photons at

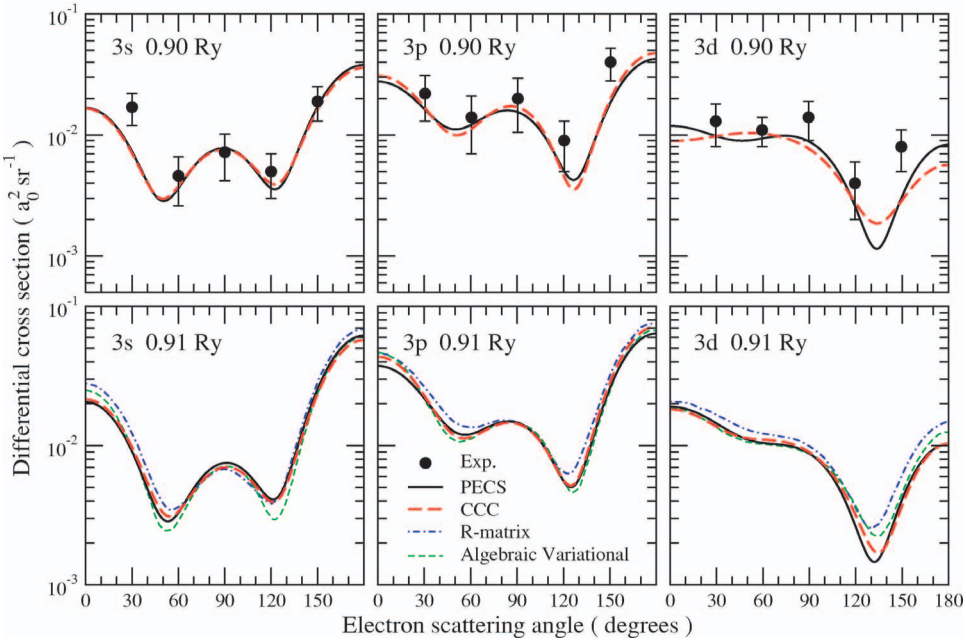

FIG. 2. (Color online) Differential cross sections for excitation of ground-state hydrogen to separate 3*s*, 3*p*, and 3*d* states for incident energies of 0.90 and 0.91 Ry. Present measurements and PECS and CCC calculations are compared with the *R*-matrix and algebraic variational calculations of Ratnavelu *et al.* [10].

12.24 eV. The 2*p* and 3*p* excitation thresholds were clearly evident, and the relative Lyman-alpha to Lyman-beta transmissions were measured.

The tests made to ensure the validity of the measurements were extensive and generally followed the procedure of [20] and references therein. All of those tests were routinely repeated to ensure the reliability, precision, and absolute accuracy of the cross sections. An absolute cross section was determined from the excitation function at 12.24 eV via the 3*p* data [17], the ratio of inelastic to elastic data, and the ratio of hydrogen to helium in the "gas flow" method [20]. Detailed discussions of the experimental uncertainties have

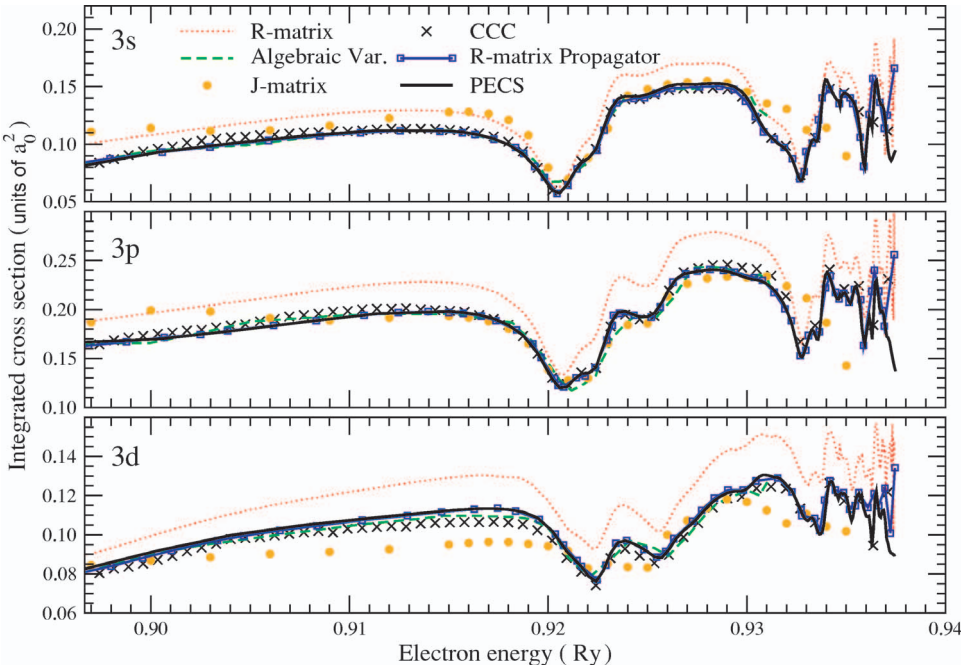

FIG. 3. (Color online) Integrated cross sections for electron-impact excitation of ground-state hydrogen to separate 3*s*, 3*p*, and 3*d* states for incident energies between 0.8967 and 0.9375 Ry. Present PECS and CCC calculations are compared with *J*-matrix calculations of Konovalov and McCarthy [7], *R*-matrix and algebraic variational calculations of Fon *et al.* [9], and *R*-matrix propagator calculations of Dunseath *et al.* [11]. The PECS and *R*-matrix propagator calculations are mostly indistinguishable.

been given in earlier work. The total counting uncertainties were estimated from the dissociation fraction (3%), transmission fraction through the analyzer (3%), coincidence identification (8%), and the energy-dependent uncertainties for raw data statistics. These are in addition to the uncertainties of the elastic DCS calibration (10%), inelastic cross-section calibration (12%), and the relative gas-flow measurement (3%), which gives the total average uncertainty of about 35% shown in our figures.

IV. RESULTS

Our measurements of the differential cross sections for the $3s$, $3p$, and $3d$ final states at 0.90 Ry (12.24 eV) are presented in Fig. 2 and show good overall agreement with our PECS and CCC calculations, both in magnitude and shape. Though the standard errors of the measurements are relatively large, reflecting the technical difficulty of the experiment, the measurements provide the first test for the theoretical calculations undertaken in this region.

The PECS and CCC $3s$ calculations are almost indistinguishable and the $3p$ show only slight variations. While the $3d$ calculations have larger variations, these occur where the cross sections are smallest or contribute least (small or large angle) to the integrated cross sections. Given that the chosen energy is very close to the $n=3$ threshold, the most challenging region for theory, these differences are consistent with our estimated calculation error.

The energy chosen for the differential cross-section measurements is below the lowest energy used in previously published calculations. We have therefore included differential calculations at 0.91 Ry (12.38 eV) in Fig. 2, which corresponds to the lowest energy considered by *R*-matrix and algebraic variational methods in Ratnavelu *et al.* [10]. The PECS, CCC, and algebraic variational calculations match well, with the largest discrepancies occurring at the smallest cross sections, and while the *R*-matrix calculations have similar shape they are consistently larger.

Figure 3 compares our PECS and CCC $3s$, $3p$, and $3d$ integrated cross sections between 12.200 eV (0.8967 Ry) and 12.755 eV (0.9375 Ry) with the *J*-matrix calculations of Konovalov and McCarthy [7], *R*-matrix and algebraic variational calculations given in [9], and the *R*-matrix propagator calculations of Dunseath *et al.* [11]. The lowest energy considered is within 0.1 eV of the $n=3$ threshold, and the PECS, CCC, and algebraic variational calculations agree to within 5% over the entire energy range for all final states. The PECS and *R*-matrix propagator calculations are mostly indistinguishable and agree to within 1% (our estimated digitization accuracy of Fig. 4 in [11]) for all final states over the majority of the energy range considered.

The *R*-matrix calculations used a 15-state basis containing only physical target states with $n \leqslant 5$, and are consistently larger than algebraic variational, and present, calculations by about 15%. Fon *et al.* [9] attribute this difference to the effect of the ionization continuum on the scattering process. They also suggest that the *J*-matrix calculations are not converged to the 5% claimed by the authors, perhaps due to insufficient terms in the expansion causing oscillations in the results. Our

TABLE I. PECS and CCC integrated scattering cross sections for excitation to the $3s$, $3p$, and $3d$ final states.

	Integrated scattering cross section (units of a_0^2)					
	$3s$		$3p$		$3d$	
E_0 (eV)	PECS	CCC	PECS	CCC	PECS	CCC
12.200	0.0816	0.0812	0.1667	0.1630	0.0826	0.0792
12.250	0.0930	0.0960	0.1698	0.1751	0.0919	0.0872
12.300	0.1007	0.1058	0.1779	0.1835	0.0998	0.0978
12.350	0.1072	0.1101	0.1872	0.1943	0.1049	0.1012
12.400	0.1119	0.1127	0.1957	0.2008	0.1089	0.1039
12.450	0.1115	0.1122	0.1980	0.1985	0.1124	0.1062
12.500	0.0913	0.0938	0.1735	0.1729	0.1116	0.1054
12.510	0.0777	0.0793	0.1552	0.1549	0.1086	0.1024
12.520	0.0600	0.0597	0.1288	0.1303	0.1019	0.0970
12.530	0.0646	0.0652	0.1210	0.1242	0.0915	0.0882
12.540	0.0840	0.0853	0.1346	0.1358	0.0838	0.0811
12.550	0.0961	0.0959	0.1413	0.1402	0.0761	0.0741
12.560	0.1308	0.1281	0.1860	0.1827	0.0906	0.0881
12.570	0.1418	0.1391	0.1982	0.1946	0.0970	0.0928
12.580	0.1417	0.1393	0.1926	0.1898	0.0938	0.0893
12.590	0.1455	0.1434	0.1965	0.1934	0.0886	0.0855
12.600	0.1506	0.1470	0.2214	0.2193	0.0925	0.0897
12.610	0.1521	0.1484	0.2361	0.2380	0.1021	0.0988
12.620	0.1522	0.1483	0.2390	0.2421	0.1089	0.1060
12.630	0.1528	0.1486	0.2406	0.2455	0.1168	0.1139
12.640	0.1518	0.1476	0.2388	0.2457	0.1213	0.1186
12.650	0.1452	0.1412	0.2338	0.2428	0.1223	0.1193
12.660	0.1247	0.1218	0.2301	0.2412	0.1285	0.1237
12.670	0.1058	0.1056	0.2226	0.2344	0.1299	0.1245
12.680	0.0953	0.0986	0.2007	0.2136	0.1258	0.1235
12.690	0.0684	0.0730	0.1522	0.1672	0.1127	0.1133
12.700	0.1031	0.1056	0.1738	0.1836	0.1058	0.1063
12.702	0.1048		0.1695		0.1013	
12.704	0.1261		0.1923		0.1005	
12.706	0.1515		0.2267		0.1051	
12.708	0.1557		0.2378		0.1184	
12.710	0.1497	0.1480	0.2328	0.2408	0.1267	0.1264
12.712	0.1441		0.2230		0.1266	
12.714	0.1400		0.2135		0.1204	
12.716	0.1380		0.2107		0.1182	
12.718	0.1416		0.2131		0.1212	
12.720	0.1442	0.1446	0.2170	0.2210	0.1211	0.1172
12.722	0.1434		0.2123		0.1180	
12.724	0.1405		0.2062		0.1096	
12.726	0.1373		0.2164		0.1091	
12.728	0.1311		0.2239		0.1185	
12.730	0.1170	0.1284	0.2109	0.2241	0.1210	0.1174

TABLE I. (*Continued.*)

E_0 (eV)	Integrated scattering cross section (units of a_0^2)					
	$3s$		$3p$		$3d$	
	PECS	CCC	PECS	CCC	PECS	CCC
12.732	0.0942		0.1812		0.1201	
12.734	0.0801		0.1653		0.1118	
12.736	0.1129		0.1846		0.1092	
12.738	0.1200		0.1832		0.1035	
12.740	0.1329	0.1192	0.1963	0.1841	0.1025	0.0944
12.742	0.1552		0.2299		0.1220	
12.744	0.1379		0.2015		0.1097	
12.746	0.1339		0.1982		0.1122	
12.748	0.1204		0.1818		0.1078	
12.750	0.0938	0.1110	0.1708	0.2311	0.0956	0.1217
12.752	0.0857		0.1581		0.0906	
12.754	0.0919		0.1427		0.0895	

calculations support these conclusions and we will not consider the *J*-matrix results further. The *R*-matrix propagator calculations [11] retained 90 box states in their close-coupling expansion, of which 55 have positive energies, and consequently the effect of the continuum was accounted for.

Below 0.93 Ry, the remaining five calculations exhibit the same resonance shapes and positions. Above 0.93 Ry, significant structure is evident, but the algebraic variational calculations did not extend into this region and the energy spacing of our CCC calculations was not fine enough to reveal the resonance structures. Though the *R*-matrix calculations continue to overestimate the cross sections in this region, the PECS, *R*-matrix, and *R*-matrix propagator calculations all show the same resonance structures.

There is, however, an extremely small region beginning 0.0005 Ry (7 meV) below the $n=4$ threshold where the structure of the *R*-matrix, *R*-matrix propagator, and PECS calculations differ. While the PECS calculations are relatively smooth in this region, both *R*-matrix calculations show one or two large resonance peaks. There is expected to be a series of Feshbach resonances in this region, whose widths become increasingly narrower and where the average size of the H^- state associated with the resonance becomes increasingly larger (see Bylicki and Nicolaides [21,22]). The H^- states associated with the "missing" resonances are most likely not contained within the grid size used for our PECS calculations, and finding extremely narrow resonances becomes problematic when separate calculations are needed at each energy. The *R*-matrix methods, on the other hand, solve for all energies simultaneously and would detect fine resonance structures more readily. There is, however, disagreement between the *R*-matrix and *R*-matrix propagator methods in this region, though the wider energy spacing of the *R*-matrix propagator results makes definitive conclusions difficult. It is possible that none of the results presented are fully converged in this narrow region near the $n=4$ threshold.

To facilitate future comparisons, we have included a subset of our PECS and CCC integrated scattering cross-section results in Table I.

V. CONCLUSIONS

We have demonstrated that the PECS method can efficiently calculate integrated and differential scattering cross sections below the ionization threshold. The PECS calculations are in excellent accord with CCC and algebraic variational [9] calculations for electron-impact scattering to the separate $3s$, $3p$, and $3d$ states of hydrogen at energies below the $n=4$ threshold. Furthermore, PECS was able to accurately represent the resonance structures for energies to within 7 meV of the $n=4$ threshold.

It should be noted that the CCC method provided benchmark calculations [23] (along with *R*-matrix with pseudostates and intermediate energy *R*-matrix methods) for the integrated cross sections for $2s$ and $2p$ excitation below the $n=3$ threshold that matched the detailed measurements of [24]. Therefore, the good agreement of the present PECS and CCC calculations, along with the very close agreement of PECS with the *R*-matrix propagator calculations of Dunseath *et al.* [11], provides strong evidence of the efficacy of the PECS method below the ionization threshold.

Our measurements of the separate $3s$, $3p$, and $3d$ differential cross sections at 12.24 eV, while technically challenging and with relatively large error estimates, validate the theoretical calculations undertaken in this difficult region.

ACKNOWLEDGMENTS

We would like to thank Kuru Ratnavelu for providing tabulated *R*-matrix results, and acknowledge the Australian Research Council and Australian Partnership for Advanced Computing for research funding and supercomputing facilities. I.B. gratefully acknowledges the Maui High Performance Computer Center and ISA Technologies for providing access to their IBM P690 computer in support of this project.

[1] T. N. Rescigno, M. Baertschy, W. A. Isaacs, and C. W. McCurdy, Science **286**, 2474 (1999).
[2] P. L. Bartlett, A. T. Stelbovics, and I. Bray, J. Phys. B **37**, L69 (2004).
[3] P. L. Bartlett and A. T. Stelbovics, Phys. Rev. Lett. **93**, 233201 (2004).
[4] J. F. Williams, P. L. Bartlett, and A. T. Stelbovics, Phys. Rev. Lett. **96**, 123201 (2006).
[5] J. F. Williams, P. L. Bartlett, I. Bray, A. T. Stelbovics, and A. G. Mikosza, J. Phys. B **39**, 719 (2006).

[6] P. L. Bartlett, A. T. Stelbovics, G. M. Lee, and I. Bray, J. Phys. B **38**, L95 (2005).
[7] D. A. Konovalov and I. E. McCarthy, J. Phys. B **27**, L741 (1994).
[8] Y. D. Wang and J. Callaway, Z. Phys. D: At., Mol. Clusters **30**, 141 (1994).
[9] W. C. Fon, K. Ratnavelu, Y. D. Wang, J. Callaway, and K. M. Aggarwal, J. Phys. B **28**, L191 (1995).
[10] K. Ratnavelu, Y. D. Wang, W. C. Fon, J. Callaway, and K. M. Aggarwal, J. Phys. B **29**, 2561 (1996).
[11] K. M. Dunseath, M. Terao-Dunseath, M. L. Dourneuf, and J.-M. Launay, J. Phys. B **32**, 1739 (1999).
[12] P. L. Bartlett and A. T. Stelbovics, Phys. Rev. A **69**, 022703 (2004).
[13] R. K. Peterkop, *Theory of Ionization of Atoms by Electron Impact* (Colorado Associated University Press, Boulder, CO, 1977).
[14] I. Bray and A. T. Stelbovics, Phys. Rev. A **46**, 6995 (1992).
[15] I. Bray, K. Bartschat, and A. T. Stelbovics, Phys. Rev. A **67**, 060704(R) (2003).
[16] R. W. van Boeyen and J. F. Williams, Rev. Sci. Instrum. **76**, 063303 (2005).
[17] J. F. Williams, M. Kumar, and A. T. Stelbovics, Phys. Rev. Lett. **70**, 1240 (1993).
[18] S. Chwirot and J. Slevin, J. Phys. B **20**, 3885 (1987).
[19] M. Kumar, A. T. Stelbovics, and J. F. Williams, J. Phys. B **26**, 2165 (1993).
[20] J. F. Williams, J. Phys. B **14**, 1197 (1981).
[21] M. Bylicki and C. A. Nicolaides, Phys. Rev. A **61**, 052508 (2000).
[22] M. Bylicki and C. A. Nicolaides, Phys. Rev. A **61**, 052509 (2000).
[23] K. Bartschat, I. Bray, P. G. Burke, and M. P. Scott, J. Phys. B **29**, 5493 (1996).
[24] J. F. Williams, J. Phys. B **21**, 2107 (1988).